ACS Catalysis

pubs.acs.org/acscatalysis Research Article

Redox Potential as a Predictor of Polyethylene Branching Using Nickel α-Diimine Catalysts

Alicia M. Doerr, Matthew R. Curry, Robert C. Chapleski, Justin M. Burroughs, Elizabeth K. Lander, Sharani Roy,* and Brian K. Long*

Cite This: ACS Catal. 2022, 12, 73–81 Read Online

ACCESS | Metrics & More | Article Recommendations | Supporting Information

ABSTRACT: The ability to control polyethylene branching density is of great interest as a means by which a polymer's thermomechanical properties may be tailored. One particularly interesting way in which this can be achieved is by altering the electronic characteristics of Pd- and Ni-based α-diimine catalysts through the inclusion of electron-withdrawing or electron-donating substituents onto the ligand scaffold; however, a few critical fundamental studies are absent from the literature. These include a systematic examination of electronic perturbations of Ni-based α-diimine catalysts, as well as how placement of donating or withdrawing substituents on the backbone versus *N*-aryl moieties of the α-diimine ligand framework impact polymer topology. In addition, no method currently exists by which the polymer topology may be predicted based on an intrinsic characteristic of the (pre)catalyst or ligand without requiring extensive polymerization studies. Herein, we use both experimental and computational methods to understand how the placement of electron-donating or electron-withdrawing substituents on Ni α-diimine catalysts affects PE branching density, and compare those results to the analogous unsubstituted catalyst. We will show that inclusion of electron-withdrawing substituents decreases resultant PE branching density, whereas electron-donating substituents exhibit little to no change in PE branching density. Finally, we will show that as the placement and identity of donating or withdrawing substituents are varied, so too is the redox half-wave potential ($E_{1/2}$) of the precatalysts, which can be used to generate a predictive curve by which PE branching density may be estimated for other substituted Ni-based α-diimine catalysts without the need for extensive polymerization studies.

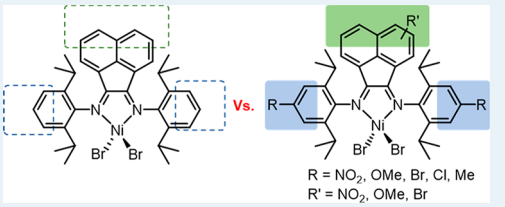

KEYWORDS: *nickel, α-diimine, polyethylene, branching, redox potential, density functional theory*

INTRODUCTION

The production of consumer-based plastics is largely dominated by synthetic, petroleum-based polymers that are produced on the scale of billions of pounds annually.[1] Pre-eminent examples include polyolefins whose widespread usage stems from their remarkable low cost and exceptional thermomechanical properties that may be fine-tuned via precise control over polymeric microstructure and topology. Such attributes ensure that polyolefin-based materials are attractive candidates for a plethora of applications.[2−11]

A polyolefin of particular interest to this study is polyethylene (PE), which is routinely synthesized using heterogeneous or homogeneous transition metal catalysts via a coordination−insertion polymerization mechanism. When early transition-metal-based heterogeneous or homogeneous catalysts are used, such as those containing Ti, Zr, or Hf, the microstructure and thermomechanical properties of the resultant PE may be altered via copolymerization of ethylene and higher α-olefins. However, reports by Brookhart and co-workers demonstrated that Ni- and Pd-based α-diimine catalysts can produce high-molecular-weight, branched PE using ethylene as the sole monomeric feedstock.[12,13] Therein, PE branching occurs due to the propensity of these Ni- and Pd-based catalysts to migrate along the growing polymer chain via a process known as "chain walking."[14,15]

Following these seminal reports of Ni- and Pd-based α-diimine catalysts, multiple methods to modulate PE topology have since been reported.[12,15−17] For example, Guan and co-workers found that PE branching could be modulated as a function of ethylene pressure when using Pd-based α-diimine catalysts. Therein, polymerizations conducted under high ethylene feed pressures resulted in more linear PE, whereas low ethylene pressures resulted in more highly branched materials. This difference in branching was attributed to the relative rates of ethylene coordination and insertion to that of β-hydride elimination and reinsertion (chain walking).[15] Alternatively, Brookhart and co-workers found that changes in polymerization temperature could similarly modulate branching density, wherein elevated reaction temperatures

Received: August 11, 2021
Revised: November 24, 2021
Published: December 10, 2021

https://doi.org/10.1021/acscatal.1c03646
ACS Catal. 2022, 12, 73−81

were found to produce PE with increased branching density relative to analogous polymerizations performed at lower temperatures.[16]

In addition to changes in reaction parameters (e.g., ethylene feed pressure and reaction temperature), changes in α-diimine ligand structure are also known to influence PE branching. Changes in α-diimine ligand design that have been shown to alter PE branching include α-diimine backbone structure,[12,17,18] steric parameters,[5,12,17,19−23] and electronic effects.[5,12,17,21,24−42] Salient examples include studies by Guan and co-workers, who showed that placement of electron-withdrawing (EW) substituents on the *N*-aryl moieties of Pd-based α-diimines produced higher degrees of PE branching, whereas catalysts bearing electron-donating (ED) substituents produce more linear PE under identical polymerization conditions.[34] They hypothesized that this change in branching content arises due to changes in the σ-donating ability of the ligand, which, in turn, alters the Lewis acidity of the active metal center and the rate of chain walking relative to that of coordination and insertion.[28,29,34,43] Chen and co-workers showed that the placement of ED methoxy (−OMe) substituents on the acenaphthene backbone moiety of Pd- and Ni-based α-diimine catalysts may also influence PE branching. More specifically, Ni-based catalysts bearing ED methoxy substituents produced PE with increased branching density, compared to their unsubstituted analogue, under identical polymerization conditions. Conversely, analogous Pd-based catalysts bearing methoxy substituents produced only a negligible decrease in PE branching density, compared to the unsubstituted analogue.[42]

Although the above-mentioned reports provide tremendous insight into the relationship between ligand-based electronic perturbations and polymerization behavior, several fundamental gaps remain. First, comprehensive studies designed to elucidate the relationship between ligand-based electronic modifications of Ni-based α-diimine catalysts (both EW and ED substituents) and PE branching density have not been reported. Second, systematic studies comparing placement of EW and ED substituents on the acenaphthene-based backbone versus placement of those same substituents on the *N*-aryl moieties of α-diimine ligands are absent from the literature. Lastly, we noted that the trends observed in most prior studies[5,18,21,27,30,34−36,38,39,41,42] were determined experimentally, requiring the iterative synthesis of multiple discrete catalyst and ligand species, as well as extensive polymerization studies. We envisioned that if PE branching density could be predicted based on catalyst structure or intrinsic catalyst and/or ligand characteristics, without requiring extensive polymerization studies and/or catalyst syntheses, that the selection and design of future catalytic species may be greatly accelerated.

To address these issues, we herein experimentally and computationally elucidate the relationship between PE branching density and placement of EW or ED substituents about the (a) acenaphthene backbone, (b) *N*-aryl moieties, and (c) both acenaphthene backbone and *N*-aryl moieties of Ni-based α-diimine catalysts. These results were compared to those obtained using the prototypical unsubstituted Ni α-diimine catalyst **1** (Figure 1). We will demonstrate that as ligand substituent placement and identity are varied, so too is the redox potential ($E_{1/2}$) of the precatalyst, revealing a linear relationship between catalyst $E_{1/2}$ and PE branching density. These experimental results agree well with computational results obtained in parallel and were used to generate a calibration curve relating PE branching to catalyst $E_{1/2}$. Finally, we demonstrate that this calibration curve can be used to predict PE branching density produced for other unique, substituted Ni-based α-diimine catalysts without the need to conduct iterative polymerizations.

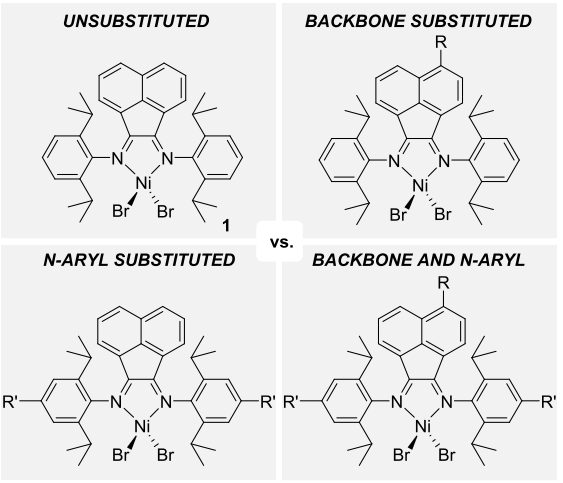

Figure 1. Unsubstituted Ni-based α-diimine precatalyst **1**, compared to Ni-based α-diimine derivatives bearing EW/ED substituents on either the acenaphthene backbone, the *N*-aryl moieties, or on both the acenaphthene backbone and *N*-aryl moieties.

RESULTS AND DISCUSSION

Unsubstituted and substituted acenaphthoquinone and aniline synthons were either purchased from commercial sources or synthesized according to modified literature procedures.[42,44−49] Unexpectedly, the nitration of acenaphthoquinone using HNO_3 in H_2SO_4 yielded an isomeric mixture of 5-nitroacenaphthoquinone and 4-nitroacenaphthoquinone, though prior reports did not discuss the formation or separation of such isomers.[46−49] However, the two nitrated isomers were readily separated via silica gel flash column chromatography to yield pure 5-nitroacenaphthoquinone, which was targeted for our subsequent studies. Ligands **L1**−**L7** were either obtained via condensation of substituted anilines with corresponding acenaphthoquinone derivatives using either formic acid in methanol (**L1**, **L2**, **L5**, **L7**), or by refluxing in toluene with catalytic *p*-toluene sulfonic acid in a Soxhlet extractor containing 4 Å molecular sieves (**L3**, **L4**, **L6**) (see Scheme 1).[13,46−49]

Ligands **L1**−**L7** were metalated using $Ni(DME)Br_2$ to produce precatalysts **1**−**7**, respectively, following previous literature procedures.[24] Precatalysts **1**−**7** were characterized using standard analytical techniques and the structures of complexes **2**, **5**, and **7** were confirmed by single-crystal X-ray diffraction. Crystallographic quality crystals of **2** and **7** were produced via slow vapor diffusion of pentane into a saturated DCM solution, whereas complex **5** was crystallized by layering DCM with pentane. X-ray analysis revealed that precatalysts **2** and **7** were dimeric in the solid state, as has been observed for other α-diimine precatalysts.[13,24] Conversely, **5** was monomeric in the solid state and adopts a tetrahedral geometry about the Ni-center (Figures S66−S68 in the Supporting Information). Numerous attempts were made to produce X-ray crystallographic quality crystals of precatalysts **3**−**4** and **6**, although we were unsuccessful.

https://doi.org/10.1021/acscatal.1c03646
ACS Catal. 2022, 12, 73−81

Scheme 1. Synthesis of Precatalysts 2−7[a]

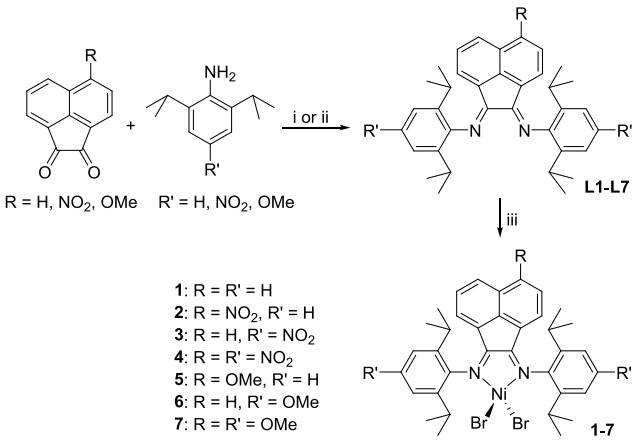

[a](i) formic acid, MeOH, Δ; (ii) *p*-toluene sulfonic acid, toluene, Δ; (iii) Ni(DME)Br_2, DCM (see the Supporting Information).

The ethylene polymerization activities of precatalysts **1**−**7** were evaluated under a constant ethylene feed pressure (15 psi relative to atmospheric pressure) using PMAO-IP as an activator (Table 1). All catalysts were active for the polymerization of ethylene, yielding 1.1−2.6 g of PE with molecular weights ranging from M_n = 104−239 kg/mol and dispersities ranging from $Đ$ = 1.32−2.81. Furthermore, all polymerizations remained homogeneous prior to quenching (no precipitation of polymer was observed), which might have otherwise adversely impacted our results. PE branching densities were measured via ^{1}H NMR spectroscopy,[50] wherein prototypical unsubstituted catalyst **1** yielded PE with 106 ± 2 branches/1000 carbons. In contrast, catalyst **2**, which incorporates an EW nitro substituent onto the acenaphthene backbone, produced PE with 66 ± 2 branches/1000 carbons. Placement of EW nitro substituents on the *N*-aryl moieties (**3**) and both the acenaphthene backbone and the *N*-aryl moieties (**4**) further decreased the PE branching density to 43 ± 3 and 49 ± 2 branches/1000 carbons, respectively.

Table 1. Polymerization of Ethylene using Catalysts 1−7[a]

catalyst	yield (g)	M_n[b] (kg/mol)	$Đ$[b]	B[c]
1	2.6	104	1.91	106 (± 2)
2	2.2	168	2.81	66 (± 2)
3	1.4	239	2.59	43 (± 3)
4	1.1	239	2.76	49 (± 2)
5	1.6	211	1.32	109 (± 1)
6	2.2	239	1.68	102 (± 3)
7	1.6	189	1.70	115 (± 1)

[a]Polymerization conditions: 15 psi (relative to atmospheric pressure) ethylene, 0.01 mmol precatalyst, 0.92 mmol PMAO-IP, 148 mL toluene, 2 mL DCM, 30 min with a constant ethylene feed pressure, no precipitation of polymer was observed during the polymerization. [b]Determined using triple detection gel permeation chromatography at 140 °C in 1,2,4-trichlorobenzene. [c]B = branches/1000 carbons, determined by ^{1}H NMR at 100 °C in $C_2D_2Cl_4$,[50] values are reported as averages over multiple polymerization trials and error is reported as one standard deviation.

The significant decrease in PE branching density observed for nitro-substituted catalysts **2**−**4**, compared to unsubstituted catalyst **1**, suggests that inclusion of EW substituents onto the α-diimine ligand scaffold generally decreases the catalyst's propensity to undergo chain walking prior to subsequent ethylene coordination and insertion. We hypothesized that this difference may arise from the EW nature of nitro substituents that decreases the overall electron density of the active metal center, thereby promoting subsequent ethylene coordination. These results also suggest that the placement of EW nitro substituents on the *N*-aryl moieties of the Ni-based α-diimine catalysts has a stronger effect on PE branching than monosubstitution on the acenaphthene backbone, which may either be due to their placement about the ligand framework or due to the presence of two nitro substituents on catalyst **3** and compared to one nitro on catalyst **2**.

Incorporation of electron ED methoxy substituents onto the acenaphthene backbone of catalyst **5** and onto both the backbone and *N*-aryl moieties of catalyst **7** marginally increased PE branching density to 109 ± 1 and 115 ± 1 branches/1000 carbons, respectively. Catalyst **6**, which features methoxy-substituted *N*-aryl moieties produced slightly fewer branches (102 ± 3 branches/1000 carbons) than **1**. Although these branching densities fall outside of our experimentally determined error for unsubstituted catalyst **1**, they suggest that the electron density around the active Ni-center and therefore the rate of β-hydride elimination, relative to the overall rate of ethylene coordination and insertion, is similar for catalysts **1**, **5**, and **6** and is only slightly increased for **7**.

This trend is consistent with that observed by Chen and colleagues for similar Ni-based α-diimine precatalysts bearing one or more −OMe substituents about the acenaphthene backbone.[42] Therein, they found that their precatalysts (activated with MAO) were also highly active for ethylene polymerization and yielded 2.34−2.88 g of PE with molecular weights ranging from 800 to 1120 kg/mol and dispersities ranging from $Đ$ = 2.0−2.8, albeit being conducted under different polymerization conditions than those used in this study (polymerization conditions: T_{rxn} = 20 °C, t_{rxn} = 10 min, and 9 atm of ethylene pressure). More importantly, however, they found that, when precatalyst **1** (no −OMe substituents) produced PE with a branching density of 79 branches/1000 carbons, whereas precatalysts incorporating one or more ED −OMe substituents produced PE with increased branching density of 80−91 branches/1000 carbons. Although the overall branching densities observed in this prior report are lower than those reported herein, which can be specifically attributed to the significantly higher ethylene feed pressures used (9 atm), this observed increase in branching density upon incorporation of the ED substituents onto the ligand scaffold observed by Chen is consistent with the change in branching density observed in this work.

Conversely, when our results are compared to those obtained by Guan and co-workers for Pd-based α-diimine catalysts bearing either ED or EW substituents in the para position of their *N*-aryl moieties, an opposite trend is observed.[34] Guan and co-workers reported that an unsubstituted Pd-based precatalyst produced PE with a branching density of 95 branches/1000 carbons when tested at 25 °C for 20 h, 1 atm of ethylene feed pressure, and activated using $NaBAr^F$. However, when EW substituents were appended on the ligand scaffold, the branching density increased slightly to 98−100 branches/1000 carbons. This trend in branching density upon incorporation of EW substituents is opposite that which was observed for the Ni-based α-diimine precatalysts bearing EW substituents (**2**−**4**) described in this study, wherein a decrease in branching density was observed upon

https://doi.org/10.1021/acscatal.1c03646
ACS Catal. 2022, 12, 73−81

incorporation of EW substituents. While we cannot yet explain why these trends appear to be different, we hypothesize that differential orbital interactions between the respective ligands and either a period 4 Ni-based metal center or a period 5 Pd-based metal center may play a pivotal role, suggesting that future computational investigations may be required.

Having established general trends relating ED/EW group placement to PE branching density, we then sought to determine if an intrinsic catalyst characteristic could be leveraged so as to predict PE branching density without requiring extensive polymerization studies. For example, the effects of EW and ED substituents on the reactivity or selectivity of aromatic compounds are commonly expressed using quantitative structure−activity relationships, such as the Hammett equation.[51] When PE branching densities obtained using catalysts **1**−**7** were plotted as a function of Hammett substituent parameters (Figure S64 in the Supporting Information), a general trend was observed. Therein, EW nitro-substituted catalysts (**2**−**4**) have positive Hammett substituent parameters and produce lower PE branching densities than unsubstituted catalyst **1**, whereas catalysts bearing ED methoxy substituents (**5**−**7**) have negative Hammett parameters and produce higher PE branching densities than unsubstituted catalyst **1**. However, these empirical parameters were unable to capture the effects of three important factors in our study: electron donation or withdrawal via resonance versus induction, the simultaneous presence of two or more ED or EW substituents, and differing placement of substituents about the ligand scaffold. Therefore, we sought another metric by which the electronic nature of each catalyst could be quickly measured, but that would also more accurately represent the often subtle variations in PE branching density obtained when using each catalyst.

Because placement and nature of EW and ED substituents are anticipated to alter the electronic nature of the catalyst, we hypothesized that electrochemical redox half-wave potential ($E_{1/2}$) might provide a direct correlation to branching density. To test this hypothesis, cyclic voltammetry (CV) studies were conducted for precatalysts **2**−**7**, using dichloromethane as the solvent, [nBu$_4$N][PF$_6$] (0.2 M) as the supporting electrolyte, and a scan rate of 100 mV s^{-1}, and referenced to a Fc/Fc$^+$ standard (see Figures S52, S53, and S55−S58, and Table S1, in the Supporting Information). The measured $E_{1/2}$ values of precatalysts **2**−**7** were then compared to unsubstituted precatalyst **1**, which exhibited a $E_{1/2}$ = −0.90 V (vs Fc/Fc$^+$) (Table S1). We found that when EW nitro substituents were introduced to the ligand scaffold (**2** and **3**), their $E_{1/2}$ values were −0.64 and −0.61 V (vs Fc/Fc$^+$), respectively. Conversely, when ED methoxy substituents were appended onto the ligand scaffold (**5**−**7**), their $E_{1/2}$ values are −0.94, −0.86, and −0.99 V (vs Fc/Fc$^+$), respectively, which are similar or slightly more reducing (negative) than that of unsubstituted precatalyst **1**. Attempts to measure the $E_{1/2}$ of complex **4** revealed multiple, overlapping signals of varying intensity, making determination of a single, reliable $E_{1/2}$ value difficult (Figure S55), and, therefore, this precatalyst was not included in subsequent investigations.

Plots of PE branching density as a function of measured $E_{1/2}$ for precatalysts **1**−**3** and **5**−**7** revealed a clear trend in which catalysts with more negative $E_{1/2}$ values produce more branches/1000 carbons (**5**−**7**) and catalysts with less negative $E_{1/2}$ produce less branches/1000 carbons (**2** and **3**), compared to unsubstituted catalyst **1** (Figure 2). In addition to a qualitative trend, Figure 2 shows that experimentally obtained PE branching density versus catalyst $E_{1/2}$ values can be represented by a linear function:

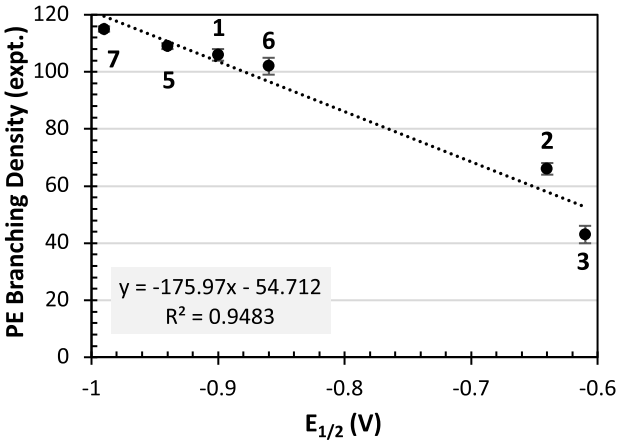

Figure 2. Plot of experimental PE branching density vs experimental $E_{1/2}$ (V) for catalysts **1**−**3** and **5**−**7**. Note: error bars are included for each data point but may not be fully visible due to data point size.

$$B = m(E_{1/2}) + c$$

where B is the number of branches per 1000 carbons, m is the slope, and c is the intercept. The slope of the linear fit shows that an increase in $E_{1/2}$ of the precatalyst by 0.1 V decreases the branching content of PE by ∼18 branches/1000 carbons. This clear, yet simple quantitative structure-branching relationship presents the opportunity to apply this linear function as a calibration curve by which the branching density of PE that would be produced using other Ni-based α-diimine (pre)-catalysts can be readily predicted by experimentally measuring precatalyst $E_{1/2}$ values, but without the need to perform extensive polymerization trials.

To better understand the mechanistic details underlying the observed trends in PE branching, as a function of added EW and ED substituents, theoretical branching densities were calculated using density functional theory (DFT) as implemented within the Gaussian 16 software.[52] The geometries and vibrational frequencies of the intermediates, transition states, and ethylene in the reaction pathways (Scheme 2) for catalysts **1**−**7** and **12** were optimized using the dispersion-corrected and range-separated hybrid exchange-correlation functional, ωB97XD,[53] in conjunction with the Ahlrichs def2svp basis set.[54] The ωB97XD functional is designed to model systems with long-range charge transfer more accurately and was chosen to appropriately describe electron transfer between the ligand substituents and the nickel center of the catalysts in our study. Initial or "guess" structures for the geometry optimizations were obtained from our previous computation of Scheme 2 for catalyst **1**.[43] Furthermore, the charge and spin multiplicity of each cationic, square-planar intermediate or transition state in the reaction pathway was set to +1 and singlet, respectively, based on the computational results of our previous work.[43] The success of a geometry optimization was verified by ensuring that all resulting vibrational frequencies were real, except for transition states, in which the single vibrational frequency along the reaction coordinate was imaginary. Following optimization, the electronic energies of the relaxed geometries were computed using the ωB97XD functional and the Ahlrichs def2svp basis

https://doi.org/10.1021/acscatal.1c03646
ACS Catal. 2022, 12, 73−81

Scheme 2. Catalytic Reaction Pathways for Ethylene Homopolymerization Using Ni-Based α-Diimine Catalysts

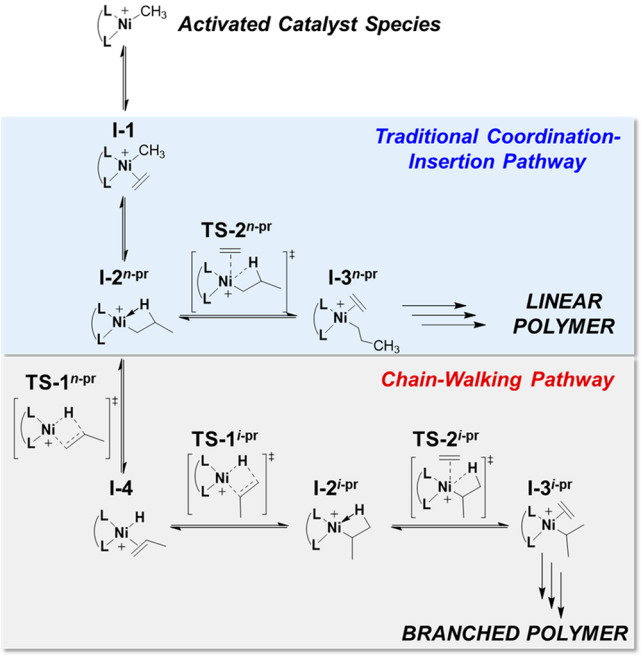

set,[54] in a polarized continuum model of the toluene solvent.[55] In the next step, the free-energy correction to the electronic energy was computed for the standard conditions of 1 atm and 298 K using the same level of theory as the geometry optimizations, i.e., ωB97XD/def2svp. Ultimately, the standard free energy of an intermediate or transition state was calculated as the sum of its electronic energy and free-energy correction. All electronic wave functions were checked for stability and vibrational frequencies of <50 cm^{-1} were not included in the calculation of free energies.

The PE branching density produced by a specific catalyst was determined from its equilibrium constant for isomerization of the square-planar catalytic intermediate (**I-3**$^{n\text{-pr}}$, Scheme 2) containing a bound ethylene ligand and an *n*-propyl ligand to the analogous complex containing an *iso*-propyl ligand (**I-3**$^{i\text{-pr}}$, Scheme 2) that results after a single chain-walking event. The equilibrium constant was derived from the standard free energy of isomerization calculated from the DFT-computed standard-free-energy difference between **I-3**$^{i\text{-pr}}$ and **I-3**$^{n\text{-pr}}$, as shown in eqs 1 and 2 in the Supporting Information. This isomerization equilibrium was hypothesized to dictate branching density based on the results of our previous computations of ethylene homopolymerization using Ni α-diimine catalysts.[43] To further test this hypothesis, we compared the branching densities that would result as a function of either thermodynamic or kinetic driving forces, and found that the observed variations in branching content were more strongly aligned with those based on thermodynamic parameters than those expected due to kinetic differences. The equations used to calculate thermodynamic branching densities, kinetic branching densities, and a comparison between both computed values are provided in eqs 1−7 and Tables S3−S5 in the Supporting Information.

Figure 3 shows the theoretical PE branching densities produced by catalysts **1**−**3** and **5**−**7**, as a function of experimentally determined $E_{1/2}$. The branching densities are presented in Table S3 in the Supporting Information. These

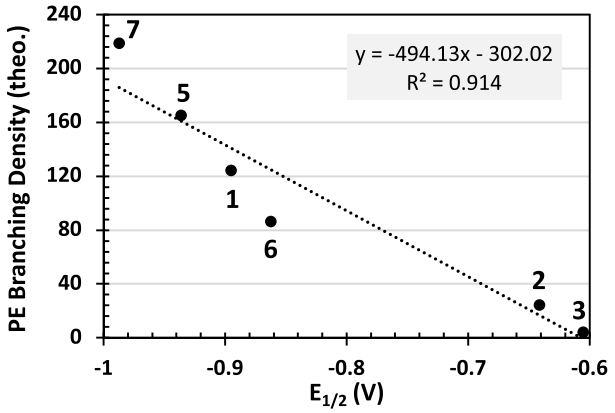

Figure 3. Plot of theoretical PE branching density versus experimental $E_{1/2}$ (V) for catalysts **1**−**3** and **5**−**7**.

results support the trend observed experimentally (Figure 2) in which catalysts with more negative $E_{1/2}$ values (**1**, **5**−**7**) are predicted to produce greater branching densities, whereas catalysts with less negative $E_{1/2}$ values (**2** and **3**) are predicted to produce lower branching densities. The theoretical PE branching density can also be fit to a linear function with a slope (m) that differs from the experimental slope by a factor of <3.

A structural analysis of the DFT results (Table S4 in the Supporting Information) reveals that EW substituents shift the isomerization equilibrium between **I-3**$^{n\text{-pr}}$ and **I-3**$^{i\text{-pr}}$ toward **I-3**$^{n\text{-pr}}$ by strengthening the Ni-ethylene and Ni-propyl interaction in **I-3**$^{n\text{-pr}}$ while concurrently weakening the Ni-propyl β-agostic interaction in **I-3**$^{i\text{-pr}}$. The Ni-ethylene interaction in **I-3**$^{i\text{-pr}}$ is unable to be strengthened by EW substituents, because of strong steric repulsion from the *iso*-propyl ligand, which significantly distorts the square planar geometry of **I-3**$^{i\text{-pr}}$ and prevents ethylene from approaching closer to Ni. Because of this repulsion, the planar angle about the Ni center in **I-3**$^{i\text{-pr}}$ is 47°, compared to 0° in a perfectly square planar complex. Overall, these geometric effects support the hypothesis that EW substituents favor ethylene coordination more than β-hydride elimination, relative to unsubstituted catalyst **1**. As shown in Table S4, ED substituents have a negligible effect on Ni-ethylene and Ni-propyl distances in **I-3**$^{n\text{-pr}}$ and, consequently, have a small effect on branching density. Furthermore, our free-energy analysis shows that changes in branching density for catalysts **5**−**7**, relative to **1**, occur partly due to the entropic penalty of binding an *n*-propyl ligand compared to an *iso*-propyl ligand.

Having established a correlation between PE branching and catalyst $E_{1/2}$, we sought to examine the predictive capabilities of this method. To do this, we synthesized five additional precatalysts (**8**−**12**; see Figure 4) with expected $E_{1/2}$ values within the range of our experimentally determined calibration curve (Figure 2). As previously discussed, synthesis of nitroacenaphthoquinone yielded two isomers, but only one of which was used for the aforementioned studies. Having also isolated pure 4-nitroacenaphthoquinone, this synthon was used to access precatalyst **8**, which enabled us to simultaneously investigate the effect that EW nitro substituent placement on the acenaphthene backbone has on PE branching density. Precatalysts bearing halide substituents (**9**−**11**) were also chosen as they were expected to exhibit $E_{1/2}$ values between those measured for complexes **2** and **3** and **5**−**7**; however, they

https://doi.org/10.1021/acscatal.1c03646
ACS Catal. 2022, 12, 73−81

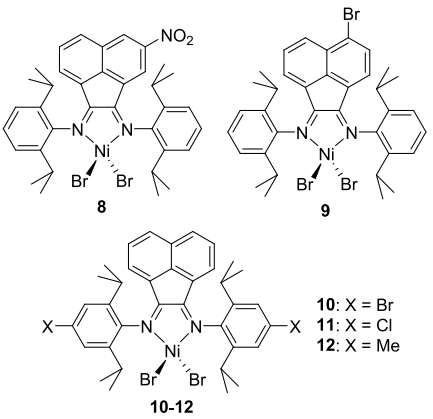

Figure 4. Structures of precatalysts **8**−**12**.

would also enable us to apply our predictive curve to substituents that are inductively EW but that may also donate electron density via the ligands π-system. Lastly, a precatalyst bearing methyl substituents (**12**) was chosen as it is also expected to be slightly ED and fall within the $E_{1/2}$ range of precatalysts **1** and **5**−**7**. Precatalysts **8**−**12** were synthesized following synthetic routes similar to those for **2**−**7** (see Supporting Information) and were all characterized using standard analytical techniques.

The $E_{1/2}$ of precatalysts **8**−**12** were measured using CV under identical conditions as **1**−**7** (see Figures S59−S63, and Table S2, in the Supporting Information). As expected, the redox potential ($E_{1/2}$) for precatalyst **8** was similar to the other nitro-substituted precatalysts ($E_{1/2}$ = −0.69 V (vs Fc/Fc$^+$)), precatalysts **9**−**11** were between those of the nitro-substituted precatalysts and the methoxy-substituted precatalysts ($E_{1/2}$ = −0.80, −0.78, and −0.79 V (vs Fc/Fc$^+$), respectively), and precatalyst **12** was within the range of the methoxy substituted precatalysts ($E_{1/2}$ = −0.87 V (vs Fc/Fc$^+$)). Using the measured $E_{1/2}$ values of precatalysts **8**−**12**, the PE branching density was then predicted using the fitting function generated by the experimental calibration curve (Figure 5, triangles), prior to performing any polymerization trials. The predicted PE branching densities were 67, 86, 83, 84, and 98 branches/1000 carbons for precatalysts **8**−**12**, respectively (see Table S2).

The ethylene polymerization activity of precatalysts **8**−**12** was then evaluated under a constant ethylene feed pressure (15 psi, relative to atmospheric pressure) using PMAO-IP as an activator (see Table S2 in the Supporting Information). Similar to the results observed when using precatalysts **1**−**7**, all polymerizations using precatalysts **8**−**12** remained homogeneous prior to quenching with methanol. The experimentally determined branching density (Figure 5, circles) when using catalysts **8** and **10** (64 ± 2 and 82 ± 1 branches/1000 carbons, respectively) were in very close agreement with predicted values. Catalysts **9** and **11** produced PE with 103 ± 4 and 79 ± 1 branches/1000 carbons, respectively, and were also within reasonable agreement with the predicted values. However, the experimental branching density obtained using catalyst **12** was significantly lower than predicted, yielding a PE with only 71 ± 3 branches/1000 carbons (versus predicted value of 98 branches/1000 carbons), and surprisingly close to the experimentally determined PE branching density obtained using catalyst **2** (66 branches/1000 carbons) that contains an EW nitro substituent on the acenaphthene backbone.

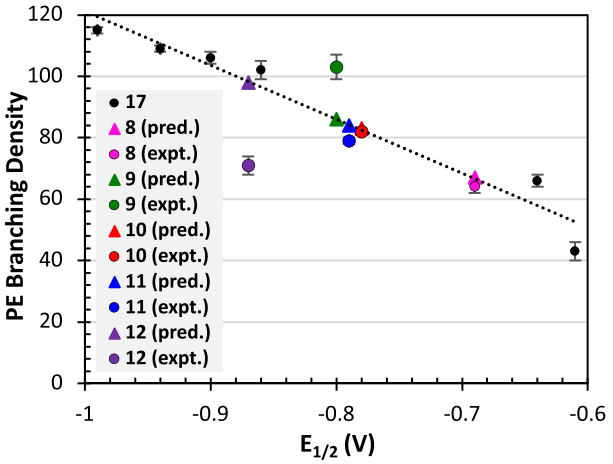

Figure 5. Experimental calibration curve with predicted (triangles) and experimental (circles) branching density (branches/1000 carbons) for **8** (pink), **9** (green), **10** (red), **11** (blue), and **12** (purple). Predicted values determined using the fit generated with the experimental calibration curve. Notes: (a) error bars are included for each experimentally measured data point, but may not be fully visible due to data point size; and (b) predicted and experimental markers for **10** coalesce.

Using DFT analysis, the theoretical branching density produced by **12** (18 branches/1000 carbons) was similarly found to be close to the theoretical branching density obtained using **2** (24 branches/1000 carbons), which differs from that which was predicted based on experimentally determined trends (Figure 2). Geometric analysis of the DFT results revealed that similar to the effects of EW nitro substituents, the ED methyl substituent shortens the Ni-ethylene interaction of **I-3**$^{n\text{-pr}}$ while weakening the β-agostic interaction between Ni and the *iso*-propyl ligand in **I-3**$^{i\text{-pr}}$, thereby shifting the isomerization equilibrium between **I-3**$^{n\text{-pr}}$ and **I-3**$^{i\text{-pr}}$ toward **I-3**$^{n\text{-pr}}$. We hypothesize that the discrepancy between PE branching densities predicted when using catalyst **12** (based on trends derived in Figure 2) and those that were experimentally measured and predicted based on DFT analysis, stems from available modes of intramolecular electron density transfer for each species. More specifically, for ED methyl substituents (i.e., catalyst **12**), this electron density transfer occurs primarily via σ-donation, whereas ED methoxy substituents transfer electron density via both σ-withdrawing and π-donation effects.

CONCLUSION

In summary, we have systematically examined how placement of EW and ED substituents on either the acenaphthene-derived backbone, *N*-aryl moieties, or both impact the degree of PE branching obtained when using Ni-based α-diimine olefin polymerization catalysts. Our results demonstrate that catalysts bearing EW nitro substituents (**2**−**4**) produce PE with decreased branching density, relative to unsubstituted catalyst **1**. In contrast, catalysts bearing ED methoxy substituents (**5**−**7**) produce PE with little to no change in PE branching density, when compared to unsubstituted **1** under identical polymerization conditions.

We also demonstrated that as the electronic nature of these Ni α-diimine catalysts are varied as a function of substituent identity (EW vs ED), number (**1** vs **2** vs **3**), and position (backbone vs *N*-aryl moiety), so too is the redox half-wavepotential ($E_{1/2}$) of those precatalysts. A plot of PE

https://doi.org/10.1021/acscatal.1c03646
ACS Catal. 2022, 12, 73−81

branching density as a function of each precatalyst's $E_{1/2}$ value revealed a linear trend in which catalysts with more negative $E_{1/2}$ values (**1**, **5**−**7**) produce PE with higher branching densities, whereas catalysts with more positive $E_{1/2}$ values (**2** and **3**) produce PE with lower branching densities.

DFT was then used to better understand the mechanistic details behind the observed modulation of PE branching density as a function of EW and ED group incorporation. The computed branching densities support our experimentally observed trend in which the incorporation of π-EW substituents decreases PE branching and incorporation of ED substituents increases PE branching. Geometric analysis of the two key intermediates in the isomerization pathway show that π-EW substituents strengthen Ni-ethylene coordination along the linear polymerization route whereas π-ED substituents have a negligible effect on Ni-ethylene coordination.

Lastly, we examined the predictive powers of the observed relationship between precatalyst $E_{1/2}$ and PE branching density through the synthesis of five additional Ni-based α-diimine catalysts (**8**−**12**). The experimental PE branching densities of catalysts **8**−**11** were found to be within good agreement of the predicted values; however, the experimentally measured PE branching density when using catalyst **12** exhibited a much lower branching density than predicted. This result was corroborated by computation, which found that the ED methyl substituents in **12** had a qualitatively similar effect on the isomerization equilibrium as the EW nitro substituents in **2**−**4**. Although we anticipate that the predictive method established herein may be used to strategically design future Ni α-diimine-based catalysts for tailored PE branching, without the need for exhaustive polymerization studies, the observed difference between predicted and experimentally measured branching densities obtained using catalyst **12** highlights a possible limitation of our predictive model. We hypothesize that the discrepancy between PE branching densities predicted for catalyst **12** (based upon trends derived in Figure 2) and those that were experimentally measured and predicted based on DFT analysis, stems from available modes of intramolecular electron density transfer for each species.

■ ASSOCIATED CONTENT

Supporting Information

The Supporting Information is available free of charge at https://pubs.acs.org/doi/10.1021/acscatal.1c03646.

Experimental procedures, NMR spectroscopy, cyclic voltammetry, GPC, DSC, and X-ray crystallography, computational methods to calculate thermodynamic branching densities and kinetic branching densities, table of computed branching densities, and table of geometric properties of reaction intermediates (PDF)

Coordinates of all structures (XYZ)

■ AUTHOR INFORMATION

Corresponding Authors

Brian K. Long − *Department of Chemistry, University of Tennessee, Knoxville, Tennessee 37996, United States;* orcid.org/0000-0002-2691-6194; Email: Long@utk.edu

Sharani Roy − *Department of Chemistry, University of Tennessee, Knoxville, Tennessee 37996, United States;* orcid.org/0000-0002-1020-482X; Email: sharani.roy@utk.edu

Authors

Alicia M. Doerr − *Department of Chemistry, University of Tennessee, Knoxville, Tennessee 37996, United States*

Matthew R. Curry − *Department of Chemistry, University of Tennessee, Knoxville, Tennessee 37996, United States*

Robert C. Chapleski − *Department of Chemistry, University of Tennessee, Knoxville, Tennessee 37996, United States;* orcid.org/0000-0001-9088-6295

Justin M. Burroughs − *Department of Chemistry, University of Tennessee, Knoxville, Tennessee 37996, United States*

Elizabeth K. Lander − *Department of Chemistry, University of Tennessee, Knoxville, Tennessee 37996, United States*

Complete contact information is available at: https://pubs.acs.org/10.1021/acscatal.1c03646

Author Contributions

All authors have given approval to the final version of the manuscript.

Notes

The authors declare no competing financial interest.

■ ACKNOWLEDGMENTS

The authors acknowledge the University of Tennessee, Knoxville, for financial support of this work. All computations were performed on the Infrastructure for Scientific Applications and Advanced Computing (ISAAC) cluster at the University of Tennessee, Knoxville.

■ ABBREVIATIONS

PE, polyethylene; EW, electron-withdrawing; ED, electron-donating; $E_{1/2}$, redox potential; CV, cyclic voltammetry

■ REFERENCES

(1) ACC Plastics Industry Producers' Statistics Group. *U.S. Resin Production & Sales 2020 vs. 2019*; American Chemistry Council, 2021; available via the Internet at:https://www.americanchemistry.com/chemistry-in-america/data-industry-statistics/statistics-on-the-plastic-resins-industry/resources/us-resin-production-sales-2020-vs-2019 (accessed November 23, 2021).

(2) Fang, J.; Sui, X.; Li, Y.; Chen, C. Synthesis of Polyolefin Elastomers from Unsymmetrical α-Diimine Nickel Catalyzed Olefin Polymerization. *Polym. Chem.* **2018**, *9*, 4143−4149.

(3) Leone, G.; Mauri, M.; Bertini, F.; Canetti, M.; Piovani, D.; Ricci, G. Ni(II) A-Diimine-Catalyzed α-Olefins Polymerization: Thermoplastic Elastomers of Block Copolymers. *Macromolecules* **2015**, *48*, 1304−1312.

(4) Lian, K.; Zhu, Y.; Li, W.; Dai, S.; Chen, C. Direct Synthesis of Thermoplastic Polyolefin Elastomers from Nickel-Catalyzed Ethylene Polymerization. *Macromolecules* **2017**, *50*, 6074−6080.

(5) Muhammad, Q.; Tan, C.; Chen, C. Concerted Steric and Electronic Effects on α-Diimine Nickel- and Palladium-Catalyzed Ethylene Polymerization and Copolymerization. *Science Bulletin* **2020**, *65*, 300−307.

(6) Na, Y.; Dai, S.; Chen, C. Direct Synthesis of Polar-Functionalized Linear Low-Density Polyethylene (LLDPE) and Low-Density Polyethylene (LDPE). *Macromolecules* **2018**, *51*, 4040−4048.

(7) O'Connor, K. S.; Watts, A.; Vaidya, T.; LaPointe, A. M.; Hillmyer, M. A.; Coates, G. W. Controlled Chain Walking for the Synthesis of Thermoplastic Polyolefin Elastomers: Synthesis, Structure, and Properties. *Macromolecules* **2016**, *49*, 6743−6751.

(8) Pierro, I.; Leone, G.; Zanchin, G.; Canetti, M.; Ricci, G.; Bertini, F. Polyolefin Thermoplastic Elastomers from 1-Octene Copolymerization with 1-Decene and Cyclopentene. *Eur. Polym. J.* **2017**, *93*, 200−211.

(9) Wang, X.; Fan, L.; Ma, Y.; Guo, C.-Y.; Solan, G. A.; Sun, Y.; Sun, W.-H. Elastomeric Polyethylenes Accessible Via Ethylene Homo-Polymerization Using an Unsymmetrical α-Diimino-Nickel Catalyst. *Polym. Chem.* **2017**, *8*, 2785−2795.
(10) Zhou, S.; Chen, C. Synthesis of Silicon-Functionalized Polyolefins by Subsequent Cobalt-Catalyzed Dehydrogenative Silylation and Nickel-Catalyzed Copolymerization. *Science Bulletin* **2018**, *63*, 441−445.
(11) Zou, C.; Dai, S.; Chen, C. Ethylene Polymerization and Copolymerization Using Nickel 2-Iminopyridine-N-Oxide Catalysts: Modulation of Polymer Molecular Weights and Molecular-Weight Distributions. *Macromolecules* **2018**, *51*, 49−56.
(12) Ittel, S. D.; Johnson, L. K.; Brookhart, M. Late-Metal Catalysts for Ethylene Homo- and Copolymerization. *Chem. Rev.* **2000**, *100*, 1169−1204.
(13) Johnson, L. K.; Killian, C. M.; Brookhart, M. New Pd(II)- and Ni(II)-Based Catalysts for Polymerization of Ethylene And.Alpha.-Olefins. *J. Am. Chem. Soc.* **1995**, *117*, 6414−6415.
(14) Guan, Z. Control of Polymer Topology by Chain-Walking Catalysts. *Chem. - Eur. J.* **2002**, *8*, 3086−3092.
(15) Guan, Z.; Cotts, P. M.; McCord, E. F.; McLain, S. J. Chain Walking: A New Strategy to Control Polymer Topology. *Science* **1999**, *283*, 2059−2062.
(16) Gates, D. P.; Svejda, S. A.; Oñate, E.; Killian, C. M.; Johnson, L. K.; White, P. S.; Brookhart, M. Synthesis of Branched Polyethylene Using (α-Diimine)Nickel(II) Catalysts: Influence of Temperature, Ethylene Pressure, and Ligand Structure on Polymer Properties. *Macromolecules* **2000**, *33*, 2320−2334.
(17) Gibson, V. C.; Spitzmesser, S. K. Advances in Non-Metallocene Olefin Polymerization Catalysis. *Chem. Rev.* **2003**, *103*, 283−316.
(18) Zhang, R.-F.; Hou, Y.-H.; Wei, X.-L.; Zhao, D.-D.; Cui, M.-M.; Zhai, F.-F.; Li, X.-L.; Liu, B.-Y.; Yang, M. Thermostable α-Diimine Nickel Complexes with Substituents on Acenaphthequinone-Backbone for Ethylene Polymerization. *Chin. J. Polym. Sci.* **2020**, *38*, 1214−1220.
(19) Liu, F.; Gao, H.; Hu, Z.; Hu, H.; Zhu, F.; Wu, Q. Poly(1-Hexene) with Long Methylene Sequences and Controlled Branches Obtained by a Thermostable α-Diimine Nickel Catalyst with Bulky Camphyl Backbone. *J. Polym. Sci., Part A: Polym. Chem.* **2012**, *50*, 3859−3866.
(20) Vaidya, T.; Klimovica, K.; LaPointe, A. M.; Keresztes, I.; Lobkovsky, E. B.; Daugulis, O.; Coates, G. W. Secondary Alkene Insertion and Precision Chain-Walking: A New Route to Semicrystalline "Polyethylene" from α-Olefins by Combining Two Rare Catalytic Events. *J. Am. Chem. Soc.* **2014**, *136*, 7213−7216.
(21) Yuan, J.; Wang, F.; Yuan, B.; Jia, Z.; Song, F.; Li, J. Highly Active Ortho-Phenyl Substituted α-Diimine Nickel(II) Catalysts for "Chain Walking Polymerization" of Ethylene: Synthesis of the Nanosized Dendritic Polyethylene. *J. Mol. Catal. A: Chem.* **2013**, *370*, 132−139.
(22) Zhong, L.; Li, G.; Liang, G.; Gao, H.; Wu, Q. Enhancing Thermal Stability and Living Fashion in α-Diimine-Nickel-Catalyzed (Co)Polymerization of Ethylene and Polar Monomer by Increasing the Steric Bulk of Ligand Backbone. *Macromolecules* **2017**, *50*, 2675−2682.
(23) Zhu, L.; Zang, D.; Wang, Y.; Guo, Y.; Jiang, B.; He, F.; Fu, Z.; Fan, Z.; Hickner, M. A.; Liu, Z.-K.; Chen, L.-Q. Insight into the Mechanism of Thermal Stability of α-Diimine Nickel Complex in Catalyzing Ethylene Polymerization. *Organometallics* **2017**, *36*, 1196−1203.
(24) Anderson, W. C.; Park, S. H.; Brown, L. A.; Kaiser, J. M.; Long, B. K. Accessing Multiple Polyethylene Grades Via a Single Redox-Active Olefin Polymerization Catalyst. *Inorg. Chem. Front.* **2017**, *4*, 1108−1112.
(25) Anderson, W. C., Jr; Rhinehart, J. L.; Tennyson, A. G.; Long, B. K. Redox-Active Ligands: An Advanced Tool to Modulate Polyethylene Microstructure. *J. Am. Chem. Soc.* **2016**, *138*, 774−7.
(26) Camacho, D. H.; Guan, Z. Designing Late-Transition Metal Catalysts for Olefin Insertion Polymerization and Copolymerization. *Chem. Commun.* **2010**, *46*, 7879−7893.
(27) Dai, S.; Sui, X.; Chen, C. Highly Robust Palladium(II) α-Diimine Catalysts for Slow-Chain-Walking Polymerization of Ethylene and Copolymerization with Methyl Acrylate. *Angew. Chem., Int. Ed.* **2015**, *54*, 9948−9953.
(28) Gasperini, M.; Ragaini, F. Method of Establishing the Lewis Acidity of a Metal Fragment Based on the Relative Binding Strengths of Ar-Bian Ligands (Ar-Bian = Bis(Aryl)-Acenaphthenequinonediimine). *Organometallics* **2004**, *23*, 995−1001.
(29) Gasperini, M.; Ragaini, F.; Cenini, S. Synthesis of Ar-Bian Ligands (Ar-Bian = Bis(Aryl)Acenaphthenequinonediimine) Having Strong Electron-Withdrawing Substituents on the Aryl Rings and Their Relative Coordination Strength toward Palladium(0) and -(II) Complexes. *Organometallics* **2002**, *21*, 2950−2957.
(30) Guo, L.; Dai, S.; Chen, C. Investigations of the Ligand Electronic Effects on Alpha-Diimine Nickel(II) Catalyzed Ethylene Polymerization. *Polymers (Basel, Switz.)* **2016**, *8*, 37.
(31) Hu, X.; Wang, C.; Jian, Z. Comprehensive Studies of the Ligand Electronic Effect on Unsymmetrical α-Diimine Nickel(II) Promoted Ethylene (Co)Polymerizations. *Polym. Chem.* **2020**, *11*, 4005−4012.
(32) Li, S.; Xu, G.; Dai, S. A Remote Nonconjugated Electron Effect in Insertion Polymerization with α-Diimine Nickel and Palladium Species. *Polym. Chem.* **2020**, *11*, 2692−2699.
(33) Liu, J.; Li, Y.; Li, Y.; Hu, N. Ethylene Polymerization by (α-Diimine)Nickel(II) Complexes Bearing Different Substituents on Para-Position of Imines Activated with Mmao. *J. Appl. Polym. Sci.* **2008**, *109*, 700−707.
(34) Popeney, C.; Guan, Z. Ligand Electronic Effects on Late Transition Metal Polymerization Catalysts. *Organometallics* **2005**, *24*, 1145−1155.
(35) Popeney, C. S.; Guan, Z. Effect of Ligand Electronics on the Stability and Chain Transfer Rates of Substituted Pd(II) α-Diimine Catalysts. *Macromolecules* **2010**, *43*, 4091−4097.
(36) Popeney, C. S.; Levins, C. M.; Guan, Z. Systematic Investigation of Ligand Substitution Effects in Cyclophane-Based Nickel(II) and Palladium(II) Olefin Polymerization Catalysts. *Organometallics* **2011**, *30*, 2432−2452.
(37) Rosar, V.; Meduri, A.; Montini, T.; Fornasiero, P.; Zangrando, E.; Milani, B. The Contradictory Effect of the Methoxy-Substituent in Palladium-Catalyzed Ethylene/Methyl Acrylate Cooligomerization. *Dalton Trans.* **2018**, *47*, 2778−2790.
(38) Sui, X.; Hong, C.; Pang, W.; Chen, C. Unsymmetrical α-Diimine Palladium Catalysts and Their Properties in Olefin (Co)Polymerization. *Mater. Chem. Front.* **2017**, *1*, 967−972.
(39) Yuan, J.; Wang, X.; Mei, T.; Liu, Y.; Miao, C.; Xie, X. An α-Diimine-Nickel(II) Catalyst Bearing an Electron-Withdrawing Substituent for Olefin Polymerization. *Transition Met. Chem.* **2011**, *36*, 433.
(40) Zhao, M.; Chen, C. Accessing Multiple Catalytically Active States in Redox-Controlled Olefin Polymerization. *ACS Catal.* **2017**, *7*, 7490−7494.
(41) Zhong, L.; Du, C.; Liao, G.; Liao, H.; Zheng, H.; Wu, Q.; Gao, H. Effects of Backbone Substituent and Intra-Ligand Hydrogen Bonding Interaction on Ethylene Polymerizations with α-Diimine Nickel Catalysts. *J. Catal.* **2019**, *375*, 113−123.
(42) Zou, W.; Chen, C. Influence of Backbone Substituents on the Ethylene (Co)Polymerization Properties of α-Diimine Pd(II) and Ni(II) Catalysts. *Organometallics* **2016**, *35*, 1794−1801.
(43) Chapleski, R. C.; Kern, J. L.; Anderson, W. C.; Long, B. K.; Roy, S. A Mechanistic Study of Microstructure Modulation in Olefin Polymerizations Using a Redox-Active Ni(II) α-Diimine Catalyst. *Catal. Sci. Technol.* **2020**, *10*, 2029−2039.
(44) Carver, F. J.; Hunter, C. A.; Livingstone, D. J.; McCabe, J. F.; Seward, E. M. Substituent Effects on Edge-to-Face Aromatic Interactions. *Chem. - Eur. J.* **2002**, *8*, 2847−2859.

https://doi.org/10.1021/acscatal.1c03646
ACS Catal. 2022, 12, 73−81

(45) Meiries, S.; Nolan, S. P. A New Synthetic Route to p-Methoxy-2,6-Disubstituted Anilines and Their Conversion into N-Heterocyclic Carbene Precursors. *Synlett* **2014**, *25*, 393−398.
(46) Mikroyannidis, J. A.; Suresh, P.; Sharma, G. D. Synthesis of a Perylene Bisimide with Acetonaphthopyrazine Dicarbonitrile Terminal Moieties for Photovoltaic Applications. *Synth. Met.* **2010**, *160*, 932−938.
(47) Sun, C.-W.; Chen, S.-C.; Fang, T.-S. Substituent Effects on the Decomposition of Chemiluminescent Tricyclic Aromatic Dioxetanes. *Luminescence* **2014**, *29*, 445−450.
(48) Wang, L.; Wang, X.; Cui, J.; Ren, W.; Meng, N.; Wang, J.; Qian, X. Preparation of Chiral Trans-5-Substituted-Acenaphthene-1,2-Diols by Baker's Yeast-Mediated Reduction of 5-Substituted-Acenaphthylene-1,2-Diones. *Tetrahedron: Asymmetry* **2010**, *21*, 825−830.
(49) Xiao, Y.; Qian, X. Novel Highly Efficient Fluoroionophores with a Peri-Effect and Strong Electron-Donating Receptors: Tict-Promoted Pet and Signaling Response to Transition Metal Cations with Low Background Emission. *Tetrahedron Lett.* **2003**, *44*, 2087−2091.
(50) Jenkins, J. C.; Brookhart, M. A Highly Active Anilinoperinaphthenone-Based Neutral Nickel(II) Catalyst for Ethylene Polymerization. *Organometallics* **2003**, *22*, 250−256.
(51) Steinfeld, J. I.; Francisco, J. S.; Hase, W. L. *Chemical Kinetics and Dynamics*; Prentice Hall: Upper Saddle River, NJ, 1999.
(52) Frisch, M. J.; Trucks, G. W.; Schlegel, H. B.; Scuseria, G. E.; Robb, M. A.; Cheeseman, J. R.; Scalmani, G.; Barone, V.; Petersson, G. A.; Nakatsuji, H.; Li, X.; Caricato, M.; Marenich, A. V.; Bloino, J.; Janesko, B. G.; Gomperts, R.; Mennucci, B.; Hratchian, H. P.; Ortiz, J. V.; Izmaylov, A. F.; Sonnenberg, J. L.; Williams; Ding, F.; Lipparini, F.; Egidi, F.; Goings, J.; Peng, B.; Petrone, A.; Henderson, T.; Ranasinghe, D.; Zakrzewski, V. G.; Gao, J.; Rega, N.; Zheng, G.; Liang, W.; Hada, M.; Ehara, M.; Toyota, K.; Fukuda, R.; Hasegawa, J.; Ishida, M.; Nakajima, T.; Honda, Y.; Kitao, O.; Nakai, H.; Vreven, T.; Throssell, K.; Montgomery Jr, J. A.; Peralta, J. E.; Ogliaro, F.; Bearpark, M. J.; Heyd, J. J.; Brothers, E. N.; Kudin, K. N.; Staroverov, V. N.; Keith, T. A.; Kobayashi, R.; Normand, J.; Raghavachari, K.; Rendell, A. P.; Burant, J. C.; Iyengar, S. S.; Tomasi, J.; Cossi, M.; Millam, J. M.; Klene, M.; Adamo, C.; Cammi, R.; Ochterski, J. W.; Martin, R. L.; Morokuma, K.; Farkas, O.; Foresman, J. B.; Fox, D. J. *Gaussian 16, Rev. C.01*; Gaussian: Wallingford, CT, 2016.
(53) Chai, J.-D.; Head-Gordon, M. Long-Range Corrected Hybrid Density Functionals with Damped Atom-Atom Dispersion Corrections. *Phys. Chem. Chem. Phys.* **2008**, *10*, 6615−6620.
(54) Weigend, F.; Ahlrichs, R. Balanced Basis Sets of Split Valence, Triple Zeta Valence and Quadruple Zeta Valence Quality for H to Rn: Design and Assessment of Accuracy. *Phys. Chem. Chem. Phys.* **2005**, *7*, 3297−3305.
(55) Scalmani, G.; Frisch, M. J. Continuous Surface Charge Polarizable Continuum Models of Solvation. I. General Formalism. *J. Chem. Phys.* **2010**, *132*, 114110.

https://doi.org/10.1021/acscatal.1c03646
ACS Catal. 2022, 12, 73−81